ACSNANO

www.acsnano.org

ARTICLE

Neutral Exciton Diffusion in Monolayer MoS_2

Shiekh Zia Uddin, Hyungjin Kim, Monica Lorenzon, Matthew Yeh, Der-Hsien Lien, Edward S. Barnard, Han Htoon, Alexander Weber-Bargioni, and Ali Javey*

Cite This: https://dx.doi.org/10.1021/acsnano.0c05305

Read Online

ACCESS | Metrics & More | Article Recommendations

ABSTRACT: **Monolayer transition metal dichalcogenides (TMDCs) are promising materials for next generation optoelectronic devices. The exciton diffusion length is a critical parameter that reflects the quality of exciton transport in monolayer TMDCs and limits the performance of many excitonic devices. Although diffusion lengths of a few hundred nanometers have been reported in the literature for as-exfoliated monolayers, these measurements are convoluted by neutral and charged excitons (trions) that coexist at room temperature due to natural background doping. Untangling the diffusion of neutral excitons and trions is paramount to understand the fundamental limits and potential of new optoelectronic device architectures made possible using TMDCs. In this work, we measure the diffusion lengths of neutral excitons and trions in monolayer MoS_2 by tuning the background carrier concentration using a gate voltage and utilizing both steady state and transient spectroscopy. We observe diffusion lengths of 1.5 μm and 300 nm for neutral excitons and trions, respectively, at an optical power density of 0.6 W cm^{-2}.**

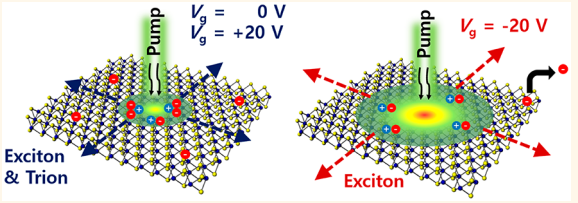

KEYWORDS: *MoS_2, exciton, trion, diffusion, transport, quantum yield*

Due to strong Coulomb interactions, photogenerated carriers in TMDC monolayers form excitons with binding energies over an order of magnitude larger than those in conventional semiconductors.[1,2] These excitons can turn into positive or negative trions in the presence of background holes or electrons, respectively.[3] Energy transport in monolayer semiconductors occurs mainly by the diffusion of these tightly bound quasiparticles. Therefore, the operation of a wide array of optoelectronic devices, such as light-emitting diodes,[4,5] solar cells,[6] and excitonic switches,[7] that utilize monolayer semiconductors is governed by exciton and trion diffusion. Understanding and manipulating the exciton diffusion in these monolayers can improve device performance and lead to the development of next-generation room-temperature excitonic technologies.

While diffusion in monolayer semiconductors has been studied extensively,[8−17] the effect of background carriers has been largely overlooked. Since almost all as-exfoliated monolayer semiconductors have some amount of unintentional doping,[18] a mixture of excitons and trions are created after photoexcitation and previous approaches have produced an averaged diffusion length of both excitons and trions. In this work, we electrostatically tune the background carrier concentration of monolayer molybdenum disulfide (MoS_2), a prototypical monolayer semiconductor, to retrieve the separated exciton and trion diffusion length. Our findings demonstrate that excitons and trions in monolayer MoS_2 have very different diffusion lengths (1.5 μm and 300 nm at a power density of 0.6 W cm^{-2}, respectively). This finding has wide implications for the design of excitonic devices utilizing monolayer semiconductors.

RESULTS AND DISCUSSION

We tune the background carrier concentration (electron and hole population densities) of the monolayer MoS_2 by varying the back-gate voltage (V_g) in a capacitor structure (Figure 1A). The schematic of the device is shown in Figure 1A, and an optical micrograph of a device is shown in the inset of Figure 1A. We also tune the photocarrier generation rate by varying the incident pump power. MoS_2 monolayers are mechanically exfoliated on top of poly(methyl methacrylate) (PMMA, 100 nm), which is spin-coated on SiO_2 (50 nm)/Si substrate. The Au contacts (thickness = 30 nm) are then transferred on the monolayer using a dry transfer technique.[18] Exciton recombination in monolayer MoS_2 was probed spatially, spectrally and temporally in an inverted fluorescence microscope (Figure 1B). Photoluminescence (PL) was excited at λ = 532 nm wavelength by either a continuous wave (CW) laser or a 100 fs

Received: June 26, 2020
Accepted: September 10, 2020
Published: September 10, 2020

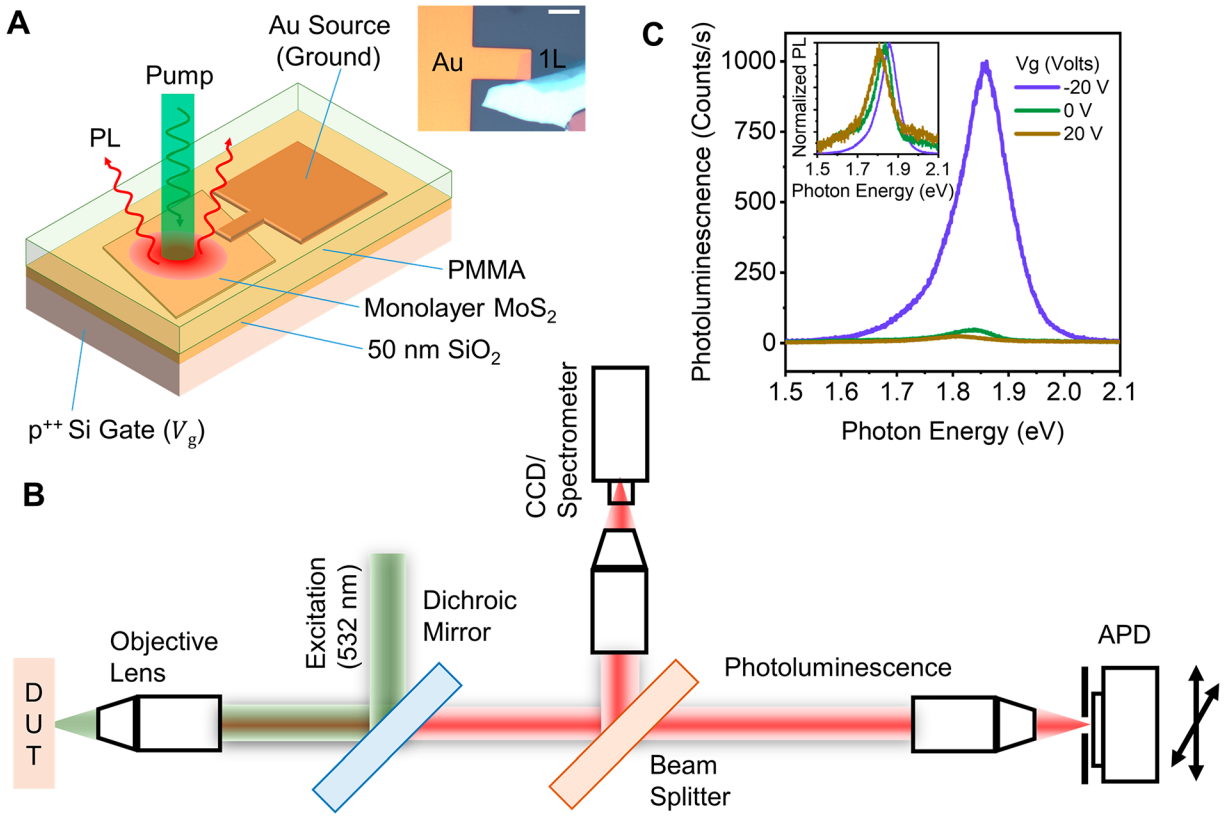

Figure 1. Neutral exciton transport in monolayer MoS_2. (A) Schematic of the device, inset shows optical micrograph of the device (scale bar = 10 μm). (B) Schematic of the exciton diffusion imaging setup. Photoluminescence excited by either pulsed or continuous wave excitation can be sent to a camera for imaging, a spectrometer for PL spectra or an APD for time-resolved single photon counting. The time-resolved APD can be scanned across the emission spot to obtain a map of emission intensity as a function of position and time. (C) PL spectra of the MoS_2 monolayer device under gate voltages V_g = −20, 0, and 20 V at the pump density of 10^2 Wcm^{-2}.

pulsed laser focused to a near-diffraction-limited spot with a full width at half-maximum (fwhm) of w_0 = 287 nm. When excited by the CW laser, the resulting PL is either imaged or sent to a spectrometer. When excited by the pulsed laser, the PL is sent to a time-resolved single photon counting detector, which is then scanned across the image to obtain a map of the time-dependent exciton density as a function of position. All measurements reported in this Article are taken at room temperature, in an ambient lab environment.

We first discuss the results of CW excitation. The PL spectra (Figure 1C) of a MoS_2 monolayer measured at V_g = −20 and 0 V show a ∼20-fold difference in the PL peak intensity at a pump power of 10^2 W cm^{-2}, with a peak energy shift of 30 meV. This difference in PL intensity and spectra has been attributed to the different photoemitting quasiparticles in the monolayer[3] (Figure 2). The time-dependent concentrations of excitons, trions and background carriers in a monolayer semiconductor are locally determined by three dynamic processes: generation, recombination and transport (Figure 2). At a specific location, exciton concentration increases if they are generated from a photon-absorption event or a trion-ionization at that location or if excitons diffuse in from surrounding points. Concurrently, exciton concentration decreases through trion formation, radiative recombination, and biexciton annihilation. Similar generation, recombination and transport processes also occur for trions. The ratio of exciton and trion concentration is determined by the local background carrier concentration, which can be controlled by the gate voltage.[18] As-exfoliated monolayer MoS_2 is electron-

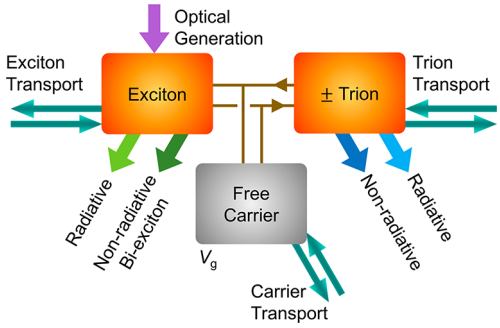

Figure 2. Local balance of various quasiparticles in monolayer MoS_2. In a differential area, exciton concentration increases by (1) generation upon absorption of a photon, (2) exciton transport into the area resulting from concentration or potential gradients, and (3) ionization of trions. Exciton concentration decreases by (1) trion formation, (2) radiative recombination, and (3) biexcitonic recombination. Similar generation and recombination processes occur for trions. The ratio of excitons and trions are controlled by the background carrier concentration, which also can drift and diffuse.

rich due to substrate-induced doping and intrinsic chalcogenide vacancies.[19] At V_g = −20 V, the background electrons are removed from the monolayer MoS_2 and it is close to intrinsic (Fermi level is at midbandgap). In this case, emission is observed primarily from neutral excitons which show high PL intensity. Positive V_g moves the Fermi level closer to the conduction band, introducing a large number of background

https://dx.doi.org/10.1021/acsnano.0c05305
ACS Nano XXXX, XXX, XXX−XXX

electrons that turn photogenerated excitons into trions. These negative trions show low PL intensity. As both neutral excitons and negative trions coexist at V_g = 0 V, previously reported diffusion lengths of as-exfoliated MoS_2 monolayers are a result of combined diffusion from both excitons and trions and do not reflect the true neutral exciton diffusion length in MoS_2.

PL images of a MoS_2 monolayer excited by a diffraction-limited CW laser at different V_g and different pump powers are shown in Figure 3. In the figure, images in the same row are

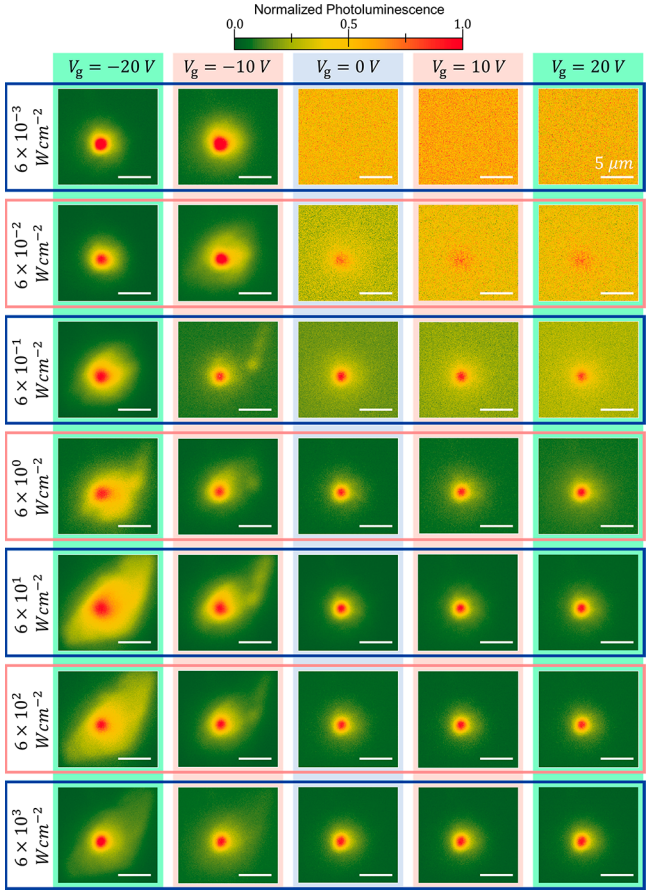

Figure 3. PL images at various pump powers and gate voltages. PL excited by a CW laser focused on a diffraction-limited spot for various pump powers and gate voltages. Images in the same row have the same pump power, and those in the same column have the same gate voltage. Scale bar is 5 μm. Radial anisotropy arises from the finite size of the monolayer.

captured at the same pump power, while images in the same column are captured at the same V_g. For the lowest pump power, we note that PL at V_g = −20 V is bright, while at V_g = 20 V it is below the noise floor, indicating neutral excitons are much brighter than the negative trions. For neutral excitons, (V_g = −20 V column) slight power dependence is observed in the measured diffusion map. Also, for all powers, neutral excitons diffuse much further than the negative trions. This is related to the difference in their effective lifetime. As neutral excitons have longer effective lifetime (~10 ns) compared to trions (~50 ps),[18] they also diffuse to a larger distance compared to trions.

Photoluminescence quantum yield (PL QY) is defined as the ratio of the number of photons the material radiates to the number of absorbed photons. We first present the PL QY of monolayer MoS_2 in Figure 4A as a function of pump power and V_g. The details of calibrated PL QY measurement and quantitative recombination kinetics at different V_g and pump have been discussed elsewhere.[18] At V_g = −20 V all photogenerated carriers create neutral excitons, as there are no excess background carriers. We note that the PL QY *versus* pump profile at V_g = −20 V has two distinct regions, indicated by different background colors in Figure 4A. At low pump the PL QY does not change with pump. PL QY reaches near unity in this linear regime. At high pump the PL QY decreases with pump power. This nonlinear droop has been attributed to the biexciton annihilation process at high exciton densities.[20] At V_g = 20 V, a large concentration of excess electrons accumulates in the monolayer, and almost all photogenerated carriers turn into negative trions (Figure 4B). Trions can nonradiatively recombine by transferring their excess energy into secondary electrons in an Auger-like process,[21] so the PL QY is low.

We now present the diffusion length of monolayer MoS_2 in Figure 4C as a function of pump power and V_g. Throughout the manuscript, we define the squared width of the diffusion pattern as

$$w^2(t) = \frac{\int d^2r\, |r|^2 I(r, t)}{\int d^2r I(r, t)} \quad (1)$$

where $I(r,t)$ is PL intensity, r is the radial coordinate, t is time, and the integrations are limited to the area of the monolayer. The steady state diffusion length (L_D) is then defined as the mean-square radius of the diffusion map deconvoluted by the laser spot size. At low pump we observe diffusion lengths of 1.5 μm and 300 nm at V_g = −20 and 20 V, respectively. At V_g= −20 V, the diffusion length shows a slight increase over 6 orders of magnitude of pump power, while at V_g = 20 V the diffusion length is low at moderate pumps and increases by ~5× at high pump. Note that we could not measure the diffusion length of trions at very low pumps due to low signal.

To extract the diffusion coefficient of neutral excitons, we extend the kinetic model of exciton recombination to incorporate diffusion. Considering only neutral excitons (at V_g = −20 V), we can write the time-dependent continuity equation as

$$\frac{\partial n_X(r, t)}{\partial t} = \nabla\cdot[D_X(n_X, t)\nabla n_X] + G(r, t) - \frac{n_X}{\tau_X} - C_{bx}{n_X}^2 \quad (2)$$

where n_X and τ_X are the neutral exciton population density and lifetime, respectively, and C_{bx} is the biexciton annihilation coefficient. Both the exciton lifetime ($\tau_X \sim 10$ ns) and biexciton annihilation coefficient ($C_{bx} \sim 3.5\ cm^2\ s^{-1}$) have been experimentally measured previously[18] and are known. At steady state, $\frac{\partial n_X}{\partial t} = 0$. We consider a Gaussian generation rate given by

$$G(r) = G_0 \exp(-2r^2/w_0^2) \quad (3)$$

where the peak G_0 is determined by pump intensity. The only unknown parameter in eq 2 is D_X. We extract an effective diffusion coefficient D_X at different pump intensity that gives the experimentally measured diffusion length shown in Figure 4C. This extraction process is done by assuming a constant diffusion coefficient and numerically solving eq 2 for exciton concentration n_X. The extracted effective diffusion coefficient at different powers is shown in Figure 4D. We note that the

https://dx.doi.org/10.1021/acsnano.0c05305
ACS Nano XXXX, XXX, XXX−XXX

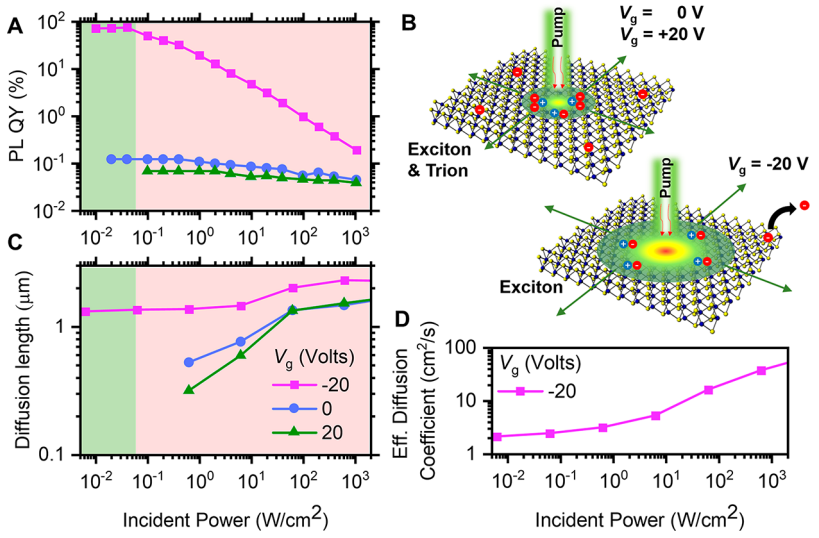

Figure 4. Diffusion of neutral excitons. (A) Pump-power dependence of the PL QY for electrostatically doped MoS_2. (B) Exciton and trion diffusion in MoS_2. (C) Diffusion length of a MoS_2 device under V_g = 0 V, V_g = −20 V, and V_g = 20 V. (D) Effective diffusion coefficient for neutral excitons in MoS_2 at different pump power.

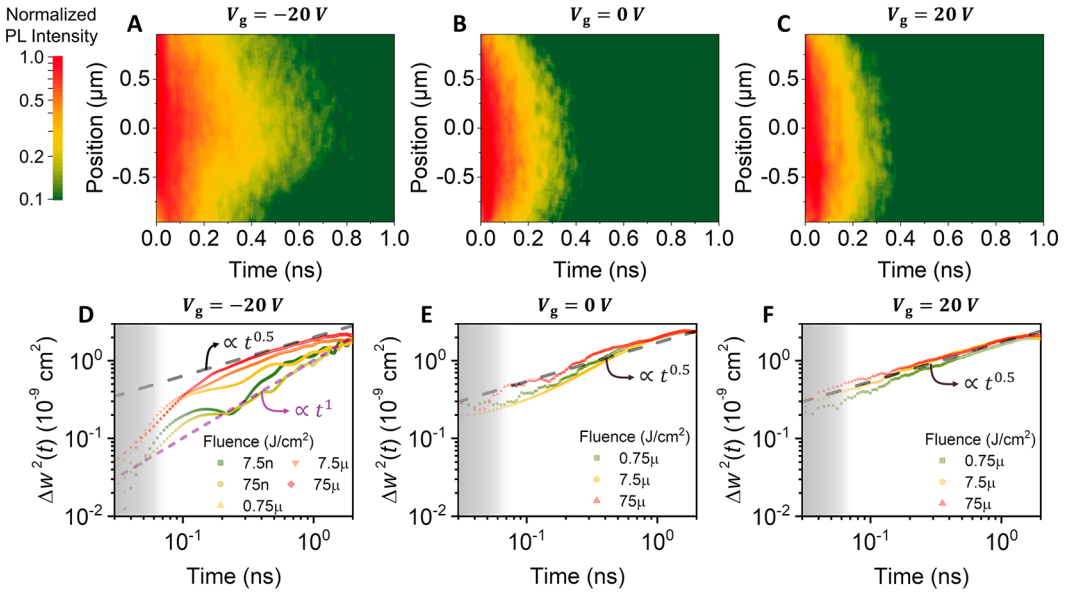

Figure 5. Temporal and spatial imaging of exciton transport in MoS_2. (A–C) Map of emission intensity as it evolves in space and time at V_g = −20, 0, and 20 V, respectively at a pump fluence of 75 μJ cm^{-2}. (D–F) Time evolution of differential squared width for various pump fluence at V_g = −20, 0, and 20 V, respectively. The instrument response function (IRF) has a fwhm of ∼50 ps, which is shown as a shaded region.

effective diffusion coefficient increases with pump power. This increase in effective diffusion coefficient has been observed in other excitonic systems such as 2D heterostructures and as-exfoliated WS_2 monolayers and is attributed to correlation driven diffusion.[8,10,22] At the lowest pump density where neutral excitons recombine completely radiatively, a diffusion length of 1.5 μm and a diffusion coefficient of 2.1 cm^{2}s^{-1} has been observed for neutral excitons.

Unlike the case of neutral excitons, extracting the trion diffusion coefficient is more complex due to its charged nature. Diffusion of trions would perturb the local charge neutrality, and the free carriers will respond to the resultant lateral electric field. Furthermore, the observed PL is a result of radiative recombination of both excitons and trions. Thus, we calculate an effective diffusion coefficient (L_D^2/τ_T^-) at V_g = 20 V using the known trion effective lifetime of τ_T^- = 50 ps[18] At a pump power density of 0.6 Wcm^{-2}, we observe a trion diffusion length of 300 nm (Figure 4C), which corresponds to an effective diffusion coefficient of 18 cm^{2}s^{-1}. This large diffusion coefficient could be a result of strong Coulomb interaction between charged trions. We also note that, at very high pump, the diffusion length at any V_g will converge to the neutral exciton diffusion length. This is because the number of trions cannot be larger than the number of background carriers, and thus once the trion population saturates, recombination and diffusion must be dominated by excitons. This explains the increase of diffusion length with pump at V_g= 20 and 0 V.

Now we discuss the results of pulsed excitation. Figure 5A–C shows the spatial and temporal evolution of the emission intensity distribution $I(r,t)$ after pulsed excitation at t = 0 at V_g = −20, 0, and 20 V, respectively, at a pump fluence of 75 μJ cm^{-2}. We can see the neutral excitons spread further in time

https://dx.doi.org/10.1021/acsnano.0c05305
ACS Nano XXXX, XXX, XXX−XXX

Table 1. Exciton Diffusion in Various Materials[a]

dimension	material	diffusion length	diffusion coefficient ($cm^2\ s^{-1}$)	refs
molecules and zero dimensional	tris(8-hydroxyquinolinato) aluminum, Alq_3	3−25 nm	$(3-2000) \times 10^{-6}$	32, 33
	spin-coated poly(*p*-phenylenevinylene) (PPV)	4−6 nm	6×10^{-4}	32, 34
	CdSe/CdS core/shell QD film	19−24 nm	2×10^{-4}	35
	cesium lead bromide perovskite nanocrystal film	200 nm	0.5	36
one dimensional	air suspended (9,8) SWCNT	290−610 nm	44	37
	micelle-encapsulated SWCNT	80−120 nm	2.5−10	38
	(6,5) single-wall carbon nanotube (SWCNT)	95−145 nm	10.7	39
	15 nm wide GaAs quantum wire (15 K)	4 μm		40
two dimensional	AlAs/GaAs coupled quantum well (200 K)	5 μm	3×10^5	41
	As-exfoliated monolayer WSe_2	500 − 1800 nm	0.6−2.2	11,42
	As-exfoliated monolayer WS_2	360 − 750 nm	0.41	8,43
	As-exfoliated monolayer $MoSe_2$	400 nm	9−15	44
	monolayer 2D perovskite	160 nm	0.06	45
three dimensional	undoped Si (11 K)	25 μm	100	46
	doped Silicon (11 K)	24 μm	11	47
	germanium (4.2 K)	900 μm	1000	48
	Cu_2O (1.2 K)	70 μm	1000	49

[a]Exciton diffusion length and diffusion coefficient of various materials. All measurements are at room temperature unless specified.

due to their considerably longer lifetime. The neutral exciton distribution variance can be obtained directly from the measured intensity distribution variance $\Delta w^2(t) = w^2(t) - w^2(0)$, which is shown in Figure 5D−F for different optical pump fluences at $V_g = -20$, 0, and 20 V, respectively. $\Delta w^2(t)$ does not depend on the width of the initial distribution created by the laser pulse. In general, the variance can be written as

$$\Delta w^2(t) = At^{\alpha} \tag{4}$$

The exponent α characterizes the type of diffusion and A is the empirically observed proportionality factor which has fractional time units. For $\alpha = 1$, we get linear diffusion. In the case of $\alpha > 1$ and $\alpha < 1$ the transport is called superdiffusive and subdiffusive, respectively, which results from the concentration dependence of the effective diffusion coefficient.[23,24] We note that in monolayer MoS_2 the nature of diffusion changes from linearly diffusive at low pump to subdiffusive at high pump (Figure 5D). This could be because of exciton−exciton interaction at high pump densities. At low fluence excitons recombine completely radiatively and diffuse linearly with $\alpha = 1$. For linear diffusion, the halved slope of $\Delta w^2(t)$ gives the diffusion coefficient. An effective diffusion coefficient of ∼1.2 $cm^2\ s^{-1}$ has been found at low fluence, which matches well with the steady state measurements. At high fluence, biexciton recombination dominates the recombination kinetics and subdiffusive ($\alpha < 1$) behavior is observed, indicative of a reaction-diffusion process. This could also be related to the relaxation of nonresonantly excited hot exciton gas by losing its excess kinetic energy[25] and further careful study is required to shed light on these mechanisms. At $V_g = 0$ and 20 V, subdiffusive behavior ($\alpha < 1$) is observed (Figure 5E, F). As previously discussed, this is a result of diffusion of both excitons and trions at high fluence.[26] The PL signal of trions is too low to measure diffusion at low pump.

Exciton diffusion length is not only of essential importance for understanding the energy transport physics in excitonic semiconductors, but also an imperative design consideration for optoelectronic applications.[27−31] The physical process of biexciton annihilation involves the diffusion of excitons and the rate of biexciton annihilation increases with diffusivity. In light emitting devices, the emission region must be located at least a diffusion length away from the injection region to avoid quenching. On the contrary, in energy harvesting devices the contacts must be closer to the absorption region to collect excitons. Materials with different diffusion coefficients can therefore be suitable for different applications. Some examples of different classes of excitonic materials with their diffusion lengths are shown in Table 1. Generally, quasi-0D systems such as molecular films and quantum dot films have very low diffusion lengths (1−50 nm) at room temperature, as the diffusion mainly occurs by site hopping.[32] One dimensional excitonic semiconductors, such as semiconducting single-wall carbon nanotube (SWCNT) have larger (∼300 nm) diffusion lengths,[36−38] depending on the chirality and dielectric environment. A two-dimensional excitonic semiconductor, such as the monolayer MoS_2 discussed here, can have an exciton diffusion length of ∼1500 nm and a trion diffusion length of 300 nm at room temperature. In a three-dimensional bulk semiconductor, strong dielectric screening generally leads to low exciton binding energy, so excitons exist only at cryogenic temperatures. At those low temperatures, they show the largest diffusion length (10−1000 μm); however, the required operating temperature limits their practical usability. Therefore, among the classes of excitonic semiconductors discussed here, two-dimensional materials such as monolayer MoS_2 achieve the highest diffusion lengths at room temperature and are particularly suitable for applications that require a large diffusion length.[27−31] Furthermore, excitons in MoS_2 achieve near-unity PL QY at room-temperature, even in the presence of defects. Exciton transport in MoS_2 can also be tuned by electrostatic doping, strain[11] and dielectric environment,[8,50] further adding to their appeal. These qualities make two-dimensional semiconductors an ideal candidate for future room-temperature excitonic devices.

CONCLUSION

In summary, we have measured the diffusion length of neutral excitons in monolayer MoS_2. The steady state exciton diffusion length is found to be between 1.5−4 μm depending on the pump intensity. Our measurements demonstrate that with increasing exciton concentration the diffusion coefficient increases and transport of neutral excitons in MoS_2 changes

https://dx.doi.org/10.1021/acsnano.0c05305
ACS Nano XXXX, XXX, XXX−XXX

from linear diffusion to subdiffusive. The diffusion coefficient of neutral excitons measured by steady state measurements and time-resolved measurements are found to be in excellent agreement. These results are direct spatial and temporal observation of isolated neutral exciton diffusion in a monolayer semiconductor, which will be invaluable for the design and characterization of systems that rely on neutral and charged exciton diffusion at room-temperature.

METHODS

Device Fabrication. TMDC monolayers are mechanically exfoliated on top of poly(methyl methacrylate) (PMMA, 100 nm), which is spin-coated on SiO_2 (50 nm)/Si substrate. MoS_2 (SPI supplies), WS_2 (HQ graphene), WSe_2 (HQ graphene) and $MoSe_2$ (HQ graphene) were mechanically exfoliated onto 50 nm SiO_2/Si p^{+2} substrates. Monolayers were identified by optical contrast. 40 nm thick Au contacts were evaporated on 280 nm SiO_2/Si, and then picked up and placed on the monolayer by a dry transfer method, using PMMA as the transfer medium. Electron-beam lithography was used to open a window in the transferred PMMA, allowing probe tip contact.

Electrical and Optical Characterization. Devices were charged from a Keithley 2410 Source Meter applied to the gate electrode, while the Au source contact was grounded. The PL QY was measured using a customized micro-PL instrument described in detail in previous study.[18,20] For steady state measurements, a green diode laser was used as the excitation source.[35] Laser source was collimated and then focused to a diffraction-limited spot by a 100× 0.95 NA objective lens. The back aperture of the objective was overfilled to ensure diffraction-limited performance. Emission from the sample was collected by the same objective and additionally magnified 5.3× for a total magnification of 530× and imaged on a camera (Andor Neo sCMOS 5.5, sensor size 16.6 mm × 14 mm, 2560 × 2160 pixels) with pixel size 6.5 μm, which provided an effective imaging pixel size of 8.63 nm. A long-pass dichroic filter and two long-pass edge filters (Semrock) were used to remove the excitation laser beam from the PL signal. To ensure no Fresnel broadening of the PL by the top PMMA, we compared the reflected laser profile from a thick reflective MoS_2 with and without top PMMA and found no significant broadening.

For time-resolved measurements, a Ti-Sapphire laser along with an OPO was used as the excitation source. The laser beam was collimated and focused by a 100× 0.95 NA objective lens. The back aperture of the objective was overfilled to ensure diffraction-limited performance. Emission from the sample was collected by the same objective and imaged on a single-mode fiber (P1-405P-FC-2, Thorlabs) attached to a translation stage (Attocube ECS series) that scanned the emission focal plane. The stage was moved in 5 μm steps corresponding to 50 nm at the sample. The signal was detected by a single-photon counting avalanche photodiode (MPD PDM-series) connected to a time-correlated single-photon counting unit (Picoharp 300). The temporal resolution was approximately 50 ps, as determined by the fwhm of the instrument response function.

We simulated the processes of exciton generation and recombination by discretizing and solving the continuity equation (eq 2) in MATLAB. The spatial grid was sampled at 5 nm distances. Time was nonuniformly sampled, denser sampling points when concentration is higher to ensure convergence.[23,24]

AUTHOR INFORMATION

Corresponding Author

Ali Javey − *Electrical Engineering and Computer Sciences, University of California, Berkeley, California 94720, United State; Materials Sciences Division, Lawrence Berkeley National Laboratory, Berkeley, California 94720, United States;* orcid.org/0000-0001-7214-7931; Email: ajavey@berkeley.edu

Authors

Shiekh Zia Uddin − *Electrical Engineering and Computer Sciences, University of California, Berkeley, California 94720, United State; Materials Sciences Division, Lawrence Berkeley National Laboratory, Berkeley, California 94720, United States;* orcid.org/0000-0002-1265-9940

Hyungjin Kim − *Electrical Engineering and Computer Sciences, University of California, Berkeley, California 94720, United State; Materials Sciences Division, Lawrence Berkeley National Laboratory, Berkeley, California 94720, United States*

Monica Lorenzon − *The Molecular Foundry, Lawrence Berkeley National Laboratory, Berkeley, California 94720, United States;* orcid.org/0000-0003-3524-9546

Matthew Yeh − *Electrical Engineering and Computer Sciences, University of California, Berkeley, California 94720, United State; Materials Sciences Division, Lawrence Berkeley National Laboratory, Berkeley, California 94720, United States*

Der-Hsien Lien − *Electrical Engineering and Computer Sciences, University of California, Berkeley, California 94720, United State; Materials Sciences Division, Lawrence Berkeley National Laboratory, Berkeley, California 94720, United States;* orcid.org/0000-0001-6774-2074

Edward S. Barnard − *The Molecular Foundry, Lawrence Berkeley National Laboratory, Berkeley, California 94720, United States*

Han Htoon − *Center for Integrated Nanotechnologies, Material Physics and Applications Division, Los Alamos National Laboratory, Los Alamos, New Mexico 87545, United States;* orcid.org/0000-0003-3696-2896

Alexander Weber-Bargioni − *The Molecular Foundry, Lawrence Berkeley National Laboratory, Berkeley, California 94720, United States*

Complete contact information is available at: https://pubs.acs.org/10.1021/acsnano.0c05305

Author Contributions

S.Z.U. and H.K. contributed equally. S.Z.U., H.K., A.W.B., and A.J. conceived the idea for the project and designed the experiments. S.Z.U., H.K., and M.L. performed optical measurements. S.Z.U., H.K., and M.Y. fabricated devices. S.Z.U., H.K., and M.L. analyzed the data. S.Z.U. performed analytical modeling. M.L., E.S.B., and A.W.B. designed and built the exciton diffusion microscope. S.Z.U., H.K., M.Y., and A.J. wrote the manuscript. All authors discussed the results and commented on the manuscript.

Notes

The authors declare no competing financial interest.

ACKNOWLEDGMENTS

Device fabrication, optical characterization, and modeling were funded by the University of California Multicampus-National Laboratory Collaborative Research and Training program (LFRP-17-477237). PL QY measurement was supported by the U.S. Department of Energy, Office of Science, Office of Basic Energy Sciences, Materials Sciences and Engineering Division, under contract DE-AC02-05CH11231, within the Electronic Materials Program (KC1201).

REFERENCES

(1) Ramasubramaniam, A. Large Excitonic Effects in Monolayers of Molybdenum and Tungsten Dichalcogenides. *Phys. Rev. B: Condens. Matter Mater. Phys.* **2012**, *86*, 115409.

(2) Zhu, B.; Chen, X.; Cui, X. Exciton Binding Energy of Monolayer WS_2. *Sci. Rep.* **2015**, *5*, 9218.
(3) Ross, J. S.; Wu, S.; Yu, H.; Ghimire, N. J.; Jones, A. M.; Aivazian, G.; Yan, J.; Mandrus, D. G.; Xiao, D.; Yao, W.; Xu, X. Electrical Control of Neutral and Charged Excitons in a Monolayer Semiconductor. *Nat. Commun.* **2013**, *4*, 1474.
(4) Ross, J. S.; Klement, P.; Jones, A. M.; Ghimire, N. J.; Yan, J.; Mandrus, D. G.; Taniguchi, T.; Watanabe, K.; Kitamura, K.; Yao, W.; Cobden, D. H.; et al. Electrically Tunable Excitonic Light-Emitting Diodes Based on Monolayer WSe_2 *p*−*n* Junctions. *Nat. Nanotechnol.* **2014**, *9*, 268−272.
(5) Lien, D. H.; Amani, M.; Desai, S. B.; Ahn, G. H.; Han, K.; He, J. H.; Ager, J. W.; Wu, M. C.; Javey, A. Large-Area and Bright Pulsed Electroluminescence in Monolayer Semiconductors. *Nat. Commun.* **2018**, *9*, 1229.
(6) Liu, Y.; Guo, J.; Zhu, E.; Liao, L.; Lee, S. J.; Ding, M.; Shakir, I.; Gambin, V.; Huang, Y.; Duan, X. Approaching the Schottky−Mott Limit in van der Waals Metal−Semiconductor Junctions. *Nature* **2018**, *557*, 696−700.
(7) Unuchek, D.; Ciarrocchi, A.; Avsar, A.; Watanabe, K.; Taniguchi, T.; Kis, A. Room-Temperature Electrical Control of Exciton Flux in a van der Waals Heterostructure. *Nature* **2018**, *560*, 340−344.
(8) Kulig, M.; Zipfel, J.; Nagler, P.; Blanter, S.; Schüller, C.; Korn, T.; Paradiso, N.; Glazov, M. M.; Chernikov, A. Exciton Diffusion and Halo Effects in Monolayer Semiconductors. *Phys. Rev. Lett.* **2018**, *120*, 207401.
(9) Cadiz, F.; Robert, C.; Courtade, E.; Manca, M.; Martinelli, L.; Taniguchi, T.; Watanabe, K.; Amand, T.; Rowe, A. C. H.; Paget, D.; Urbaszek, B.; et al. Exciton Diffusion in WSe_2 Monolayers Embedded in a van der Waals Heterostructure. *Appl. Phys. Lett.* **2018**, *112*, 152106.
(10) Zipfel, J.; Kulig, M.; Perea-Causín, R.; Brem, S.; Ziegler, J. D.; Rosati, R.; Taniguchi, T.; Watanabe, K.; Glazov, M. M.; Malic, E.; Chernikov, A. Exciton Diffusion in Monolayer Semiconductors with Suppressed Disorder. *Phys. Rev. B: Condens. Matter Mater. Phys.* **2020**, *101*, 115430.
(11) Cordovilla Leon, D. F.; Li, Z.; Jang, S. W.; Cheng, C. H.; Deotare, P. B. Exciton Transport in Strained Monolayer WSe_2. *Appl. Phys. Lett.* **2018**, *113*, 252101.
(12) Wang, J.; Guo, Y.; Huang, Y.; Luo, H.; Zhou, X.; Gu, C.; Liu, B. Diffusion Dynamics of Valley Excitons by Transient Grating Spectroscopy in Monolayer WSe_2. *Appl. Phys. Lett.* **2019**, *115*, 131902.
(13) Glazov, M. M. Phonon Wind and Drag of Excitons in Monolayer Semiconductors. *Phys. Rev. B: Condens. Matter Mater. Phys.* **2019**, *100*, 045426.
(14) Hao, S.; Bellus, M. Z.; He, D.; Wang, Y.; Zhao, H. Controlling Exciton Transport in Monolayer $MoSe_2$ by Dielectric Screening. *Nanoscale Horiz* **2020**, *5*, 139−143.
(15) Perea-Causin, R.; Brem, S.; Rosati, R.; Jago, R.; Kulig, M.; Ziegler, J. D.; Zipfel, J.; Chernikov, A.; Malic, E. Exciton Propagation and Halo Formation in Two-Dimensional Materials. *Nano Lett.* **2019**, *19*, 7317−7323.
(16) Fu, Y.; He, D.; He, J.; Bian, A.; Zhang, L.; Liu, S.; Wang, Y.; Zhao, H. Effect of Dielectric Environment on Excitonic Dynamics in Monolayer WS_2. *Adv. Mater. Interfaces* **2019**, *6*, 1901307.
(17) Raja, A.; Waldecker, L.; Zipfel, J.; Cho, Y.; Brem, S.; Ziegler, J. D.; Kulig, M.; Taniguchi, T.; Watanabe, K.; Malic, E.; Heinz, T. F.; et al. Dielectric Disorder in Two-Dimensional Materials. *Nat. Nanotechnol.* **2019**, *14*, 832−837.
(18) Lien, D. H.; Uddin, S. Z.; Yeh, M.; Amani, M.; Kim, H.; Ager, J. W.; Yablonovitch, E.; Javey, A. Electrical Suppression of All Nonradiative Recombination Pathways in Monolayer Semiconductors. *Science* **2019**, *364*, 468−471.
(19) Radisavljevic, B.; Radenovic, A.; Brivio, J.; Giacometti, V.; Kis, A. Single-Layer MoS_2 Transistors. *Nat. Nanotechnol.* **2011**, *6*, 147−150.
(20) Amani, M.; Lien, D. H.; Kiriya, D.; Xiao, J.; Azcatl, A.; Noh, J.; Madhvapathy, S. R.; Addou, R.; Santosh, K. C.; Dubey, M.; Cho, K.; et al. Near-Unity Photoluminescence Quantum Yield in MoS_2. *Science* **2015**, *350*, 1065−1068.
(21) Jha, P. P.; Guyot-Sionnest, P. Trion Decay in Colloidal Quantum Dots. *ACS Nano* **2009**, *3*, 1011−1015.
(22) Jauregui, L. A.; Joe, A. Y.; Pistunova, K.; Wild, D. S.; High, A. A.; Zhou, Y.; Scuri, G.; De Greve, K.; Sushko, A.; Yu, C. H.; Taniguchi, T.; et al. Electrical Control of Interlayer Exciton Dynamics in Atomically Thin Heterostructures. *Science* **2019**, *366*, 870−875.
(23) Crank, J. *The Mathematics of Diffusion*, 2nd ed.; Oxford University Press: Oxford, 1979.
(24) Ghez, R. A. *Primer of Diffusion Problems*, 1st ed.; Wiley: New York, 1988.
(25) Cordovilla Leon, D. F.; Li, Z.; Jang, S. W.; Deotare, P. B. Hot Exciton Transport in WSe_2 Monolayers. *Phys. Rev. B: Condens. Matter Mater. Phys.* **2019**, *100*, 241401.
(26) Rosati, R.; Perea-Causín, R.; Brem, S.; Malic, E. Negative Effective Excitonic Diffusion in Monolayer Transition Metal Dichalcogenides. *Nanoscale* **2020**, *12*, 356−363.
(27) Miller, D. A.; Chemla, D. S.; Damen, T. C.; Gossard, A. C.; Wiegmann, W.; Wood, T. H.; Burrus, C. A. Electric Field Dependence of Optical Absorption Near the Band Gap of Quantum-Well Structures. *Phys. Rev. B: Condens. Matter Mater. Phys.* **1985**, *32*, 1043.
(28) Lundstrom, T.; Schoenfeld, W.; Lee, H.; Petroff, P. M. Exciton Storage in Semiconductor Self-Assembled Quantum Dots. *Science* **1999**, *286*, 2312−2314.
(29) Hagn, M.; Zrenner, A.; Böhm, G.; Weimann, G. Electric-Field-Induced Exciton Transport in Coupled Quantum Well Structures. *Appl. Phys. Lett.* **1995**, *67*, 232−234.
(30) High, A. A.; Hammack, A. T.; Butov, L. V.; Hanson, M.; Gossard, A. C. Exciton Optoelectronic Transistor. *Opt. Lett.* **2007**, *32*, 2466−2468.
(31) High, A. A.; Novitskaya, E. E.; Butov, L. V.; Hanson, M.; Gossard, A. C. Control of Exciton Fluxes in an Excitonic Integrated Circuit. *Science* **2008**, *321*, 229−231.
(32) Mikhnenko, O. V.; Blom, P. W.; Nguyen, T. Q. Exciton Diffusion in Organic Semiconductors. *Energy Environ. Sci.* **2015**, *8*, 1867−1888.
(33) Wu, Y.; Wu, H. R.; Zhou, Y. C.; Zhan, Y. Q.; Zhou, J.; Ding, X. M.; Hou, X. Y. Excitation Energy Transfer between Tris-(8-Hydroxyquinoline) Aluminum and a Red Dye. *Appl. Phys. Lett.* **2006**, *88*, 123512.
(34) Markov, D. E.; Amsterdam, E.; Blom, P. W.; Sieval, A. B.; Hummelen, J. C. Accurate Measurement of the Exciton Diffusion Length in a Conjugated Polymer Using a Heterostructure with a Side-Chain Cross-Linked Fullerene Layer. *J. Phys. Chem. A* **2005**, *109*, 5266−5274.
(35) Lee, E. M.; Tisdale, W. A. Determination of Exciton Diffusion Length by Transient Photoluminescence Quenching and Its Application to Quantum Dot Films. *J. Phys. Chem. C* **2015**, *119*, 9005−9015.
(36) Penzo, E.; Loiudice, A.; Barnard, E. S.; Borys, N. J.; Jurow, M. J.; Lorenzon, M.; Rajzbaum, I.; Wong, E. K.; Liu, Y.; Schwartzberg, A. M.; Cabrini, S.; et al. Long-Range Exciton Diffusion in Two-Dimensional Assemblies of Cesium Lead Bromide Perovskite Nanocrystals. *ACS Nano* **2020**, *14*, 6999−7007.
(37) Moritsubo, S.; Murai, T.; Shimada, T.; Murakami, Y.; Chiashi, S.; Maruyama, S.; Kato, Y. K. Exciton Diffusion in Air-Suspended Single-Walled Carbon Nanotubes. *Phys. Rev. Lett.* **2010**, *104*, 247402.
(38) Cognet, L.; Tsyboulski, D. A.; Rocha, J. D. R.; Doyle, C. D.; Tour, J. M.; Weisman, R. B. Stepwise Quenching of Exciton Fluorescence in Carbon Nanotubes by Single-Molecule Reactions. *Science* **2007**, *316*, 1465−1468.
(39) Hertel, T.; Himmelein, S.; Ackermann, T.; Stich, D.; Crochet, J. Diffusion Limited Photoluminescence Quantum Yields in 1-D Semiconductors: Single-Wall Carbon Nanotubes. *ACS Nano* **2010**, *4*, 7161−7168.
(40) Nagamune, Y.; Watabe, H.; Sogawa, F.; Arakawa, Y. One-Dimensional Exciton Diffusion in GaAs Quantum Wires. *Appl. Phys. Lett.* **1995**, *67*, 1535−1537.

https://dx.doi.org/10.1021/acsnano.0c05305
ACS Nano XXXX, XXX, XXX−XXX

(41) Grosso, G.; Graves, J.; Hammack, A. T.; High, A. A.; Butov, L. V.; Hanson, M.; Gossard, A. C. Excitonic Switches Operating at around 100 K. *Nat. Photonics* **2009**, *3*, 577.
(42) Cadiz, F.; Robert, C.; Courtade, E.; Manca, M.; Martinelli, L.; Taniguchi, T.; Watanabe, K.; Amand, T.; Rowe, A. C. H.; Paget, D.; Urbaszek, B.; et al. Exciton Diffusion in WSe_2 Monolayers Embedded in a van-der-Waals Heterostructure. *Appl. Phys. Lett.* **2018**, *112*, 152106.
(43) Yuan, L.; Huang, L. Exciton Dynamics and Annihilation in WS_2 2D Semiconductors. *Nanoscale* **2015**, *7*, 7402−7408.
(44) Kumar, N.; Cui, Q.; Ceballos, F.; He, D.; Wang, Y.; Zhao, H. Exciton Diffusion in Monolayer and Bulk $MoSe_2$. *Nanoscale* **2014**, *6*, 4915−4919.
(45) Deng, S.; Shi, E.; Yuan, L.; Jin, L.; Dou, L.; Huang, L. Long-Range Exciton Transport and Slow Annihilation in Two-Dimensional Hybrid Perovskites. *Nat. Commun.* **2020**, *11*, 664.
(46) Tamor, M. A.; Wolfe, J. P. Drift and Diffusion of Free Excitons in Si. *Phys. Rev. Lett.* **1980**, *44*, 1703.
(47) Chen, Y. H.; Lyon, S. A. Photoluminescence and Diffusivity of Free Excitons in Doped Silicon. *IEEE J. Quantum Electron.* **1989**, *25*, 1053−1055.
(48) Sanada, T.; Ohyama, T.; Otsuka, E. Diffusion of Excitons and Electron-Hole Drops in Germanium. *Solid State Commun.* **1975**, *17*, 999−1001.
(49) Trauernicht, D. P.; Wolfe, J. P.; Mysyrowicz, A. Highly Mobile Paraexcitons in Cuprous Oxide. *Phys. Rev. Lett.* **1984**, *52*, 855.
(50) Goodman, A. J.; Lien, D.-H.; Ahn, G. H.; Spiegel, L. L.; Amani, M.; Willard, A. P.; Javey, A.; Tisdale, W. A. Substrate-Dependent Exciton Diffusion and Annihilation in Chemically Treated MoS_2 and WS_2. *J. Phys. Chem. C* **2020**, *124*, 12175−12184.

https://dx.doi.org/10.1021/acsnano.0c05305
ACS Nano XXXX, XXX, XXX−XXX